5.4 MHz dog-bone oscillating AFM probe with thermal actuation and piezoresistive detection

Zhuang Xiong, Estelle Mairiaux, Benjamin Walter, Marc Faucher, Lionel Buchaillot, Bernard Legrand

5.4 MHz DOG-BONE OSCILLATING AFM PROBE WITH THERMAL ACTUATION AND PIEZORESISTIVE DETECTION

Z. Xiong, E. Mairiaux, B. Walter, M. Faucher, L. Buchaillot, and B. Legrand
Institut d'Electronique, de Microélectronique et de Nanotechnologie – IEMN CNRS UMR8520, NAM6 group, FRANCE

ABSTRACT

We report on a new concept of Atomic Force Microscope (AFM) oscillating probes using dog-bone resonator with thermal excitation and piezoresistive detection. The resonance frequency is 5.4 MHz and the quality factor is measured about 4,000 in air. AFM images are obtained over PMMA resist sample and the force resolution deduced from the measurement is about 320 pN/Hz$^{0.5}$.

INTRODUCTION

Most of commercial Atomic Force Microscope (AFM) oscillating probes are based on micrometric cantilevers which can make measurement with piconewton force resolution in vacuum [1]. However the laser detection for amplitude measurement limits the system integration and miniaturization, and the flexural vibration of cantilever could suffer from a degradation of both resonance frequency and quality factor while operating in liquids.

In 2007 [2], we presented a concept of AFM probe using elliptic bulk mode vibration ring shaped resonator with integrated electrostatic excitation and capacitive detection. Further research work has demonstrated that such AFM probes are capable of surface imaging with a force resolution of several pN/Hz$^{0.5}$ [3-5]. The ring probe described in [5] resonates at 10 MHz with a quality factor of 1,500. Other transduction methods such as electrostatic excitation and piezoresistive detection have also been developed [6] based on the idea carried out by K.L.Phan [7].

However, the resonance frequency of ring resonator appears to reach its limit around 50 MHz and most importantly, for a future application in liquid, the electrostatic transduction are less suitable because the immersion of capacitive transducers might results in: 1. device failure due to electrical short circuit; 2. decrease of quality factor due to pinch effect in transduction gap. Therefore, an alternative transduction method should be designed to relief such problem. Here, we propose a dog-bone [8] shaped AFM probe using the thermal actuation and piezoresistive detection concept presented by Amir *et al.* [9]. Since the capacitive transduction air gaps being used in the previous devices are eliminated, it is thus expected that such new AFM probe would be more appropriate for future application in the field of *in vitro* imaging of biological samples.

DESIGN

The working principle of thermal driving and piezoresistive sensing can be described as follows: a time-varying voltage causes a temperature fluctuation in the mechanical structure. This results in a mechanical expansion/compression, which leads to a change of the material electrical resistivity. The dog-bone resonator design mainly consists of two actuator beams with two connected massif heat tank (Figure 1). By applying superimposed DC and AC voltages, temperature fluctuation created inside actuator beams will result in their alternative expansion and compression, leading to longitudinal vibration of the resonator. As for detection, the time-varying deformation of the actuator beams causes a periodic change of their electrical resistance. This piezoresistive effect results in a motional AC current passing through the device and being detected at the output port [9].

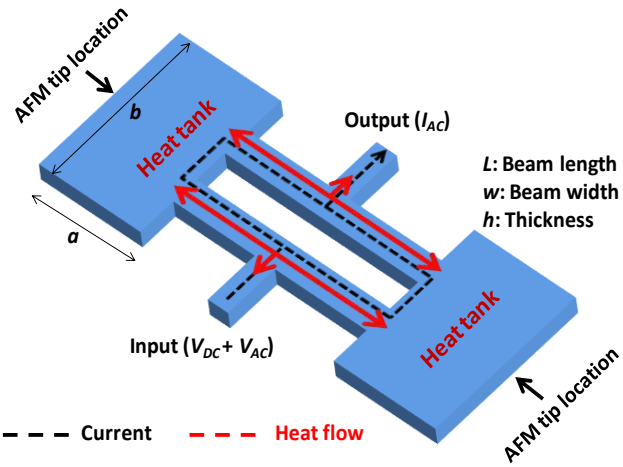

Figure 1: Schematic representation of dog-bone resonator using thermal actuation and piezoresistive detection.

The overall transfer function $H_s(\omega)$ that describes the relation between input voltage V_{AC} and output current I_{AC} can be expressed as:

$$s(\omega) = \frac{I_{AC}}{V_{AC}} = -\frac{8\kappa\alpha {V_{DC}}^2}{j\omega C_{th}\pi^2 R_p^2}\left(1 - \frac{\omega^2}{\omega_0^2} + j\frac{\omega}{Q\omega_0}\right)^{-1} \quad (1)$$

where κ is the Gauge factor of *n*-type silicon, α the thermal expansion coefficient, C_{th} the thermal capacitance of actuator beams, R_p the structure electrical resistance and Q the quality factor.

Considering the structure mechanical balance, two AFM tips are designed and located symmetrically at the outer edge of each heat tank. Moreover, to minimize the shear displacement at these locations, it is suggested to use a perfectly symmetric geometry of which the distance C1 and C2 are identical (Figure 2). The corresponding simulation results show that a mismatch in C1 and C2 will lead to significant shear displacement at the edge of heat tanks which is due to the un-balanced mass added along each side of the beam axis.

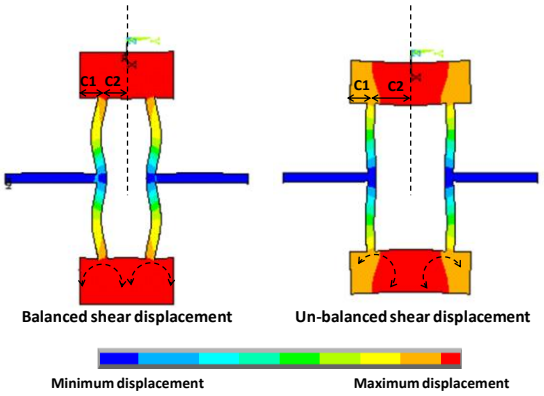

Figure 2: Modal analysis of balanced (C1=C2) and un-balanced (C1≠C2) dog-bone structure design. The shear displacement at the edge of heat tank is minimized and is ideal for AFM tip positioning.

The structure geometry designed for AFM experiment and the corresponding resonance frequency f and effective stiffness k_{eff} are listed in Table 1.

Table 1: Structure designed for AFM experiment.

Geometry (µm)	k_{eff} (N/m)	f (MHz)
L=200, w=10, a=b=100, h=2	$1.7 \cdot 10^5$	5.4

FABRICATION

Illustrated in Figure 3, the dog-bone resonator with two symmetric tips is fabricated on a n-type SOI wafer (Device layer 2 µm, BOX layer 2 µm, Handle layer 300 µm, doping level 10^{18} atoms/cm^3). The resonator layout is first patterned on the device layer by DRIE. A highly doped (10^{21} atoms/cm^3) zone is then created over the surface to obtain ohmic contact followed by deposition of Cr/Au electrical interconnects. The front side of wafer is then protected by thick resist and another DRIE is processed on the handle layer to create the opening over the back side of resonator. After removing the protection resist, the BOX layer is etched in HF and the resonator is finally released after the supercritical CO_2 drying process.

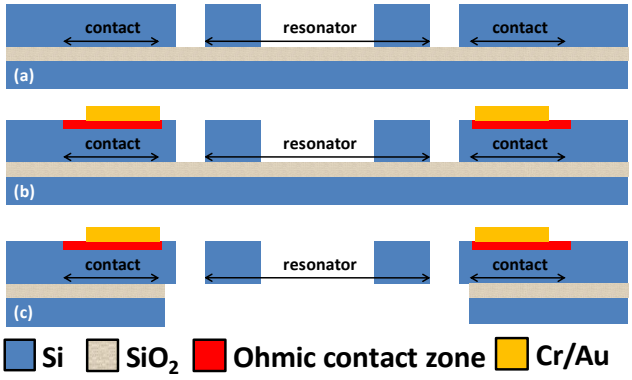

Figure 3: Fabrication process (a) DRIE etching. (b) Ion implantation and metal deposition. (c) DRIE etching and releasing.

A fabricated device is shown in Figure 4. The actuator beam is 200 µm in length and 10 µm in width. Two symmetric tips are prolonged from the 100×100 µm square heat tank. The resonator is held by the trapezoid shape anchors to enhance the support rigidity and facilitate the drain of heat flow from beam to substrate. The electrical accesses (Cr/Au) are placed close to the resonator in order to minimize the ohmic losses from input/output to actuator beams. The tip (150 µm long and 10 µm width, Figure 4b) is fabricated by DRIE and a further FIB step is required to obtain a tip apex small enough for AFM operation and satisfying lateral resolution (Figure 4c).

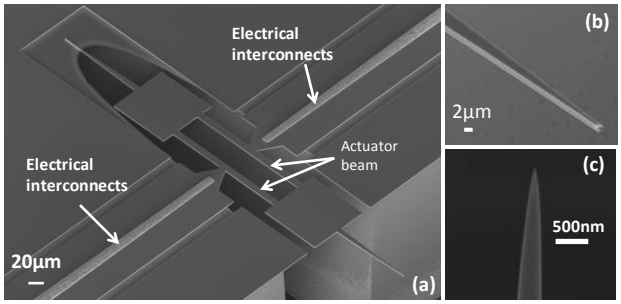

Figure 4: SEM images of (a) Overview of fabricated device. (b)Close view of the 150 µm massif tip. (c) Tip sharpened by FIB etching.

CHARACTERIZATION

Electrical measurement

The measurement principle is depicted in Figure 5. The DC bias V_{DC} is applied between anchors to bias the actuator beams and create a current I_{DC} passing through. The network analyzer (VNA) supplies an input power (this power corresponds to an AC excitation voltage V_{AC} generated over a 50 Ω resistance) at port 1 which drives the resonator to longitudinal vibration by thermal effect. The change of piezoresistance due to vibration combined with the DC bias results in an AC current I_{AC} passing through the structure and being collected at port 2 of the VNA. Besides piezoresistive current I_{AC}, the driving signal V_{AC} also passes directly across the structure electrical resistance and results in a parasitic current I_{para}. The total output signal captured is thus the superposition of I_{AC} and I_{para}.

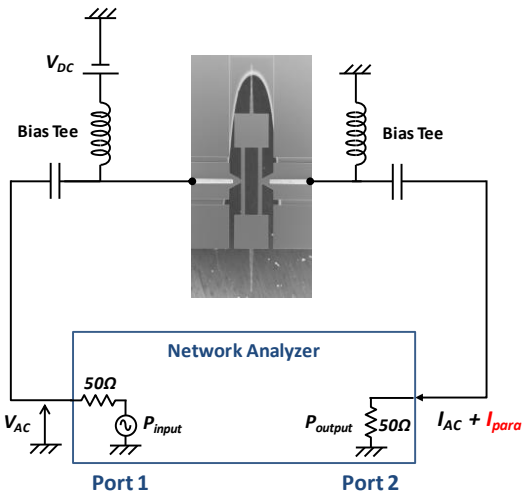

Figure 5: Schematic representation of working principle. V_{DC} is used to bias the actuator beams for piezoresistive detection. Network analyzer generates a driving signal V_{AC} and collects the output piezoresistive current I_{AC}.

Figure 6 shows the frequency response of a dog-bone AFM probe resonating around 5.47 MHz in air with different driving voltage and a fixed V_{DC} of 3 V. The structure geometry is the same as shown in Figure 4. The resonance peak is inverted and superimposed with a direct-coupling signal floor I_{para}. By transmitting the output power into current over 50 Ω, the corresponding I_{para} can be obtained (shown in Figure 6). The device electrical resistance R_p is thus the quotient of V_{AC} and I_{para} which is about 1 kΩ.

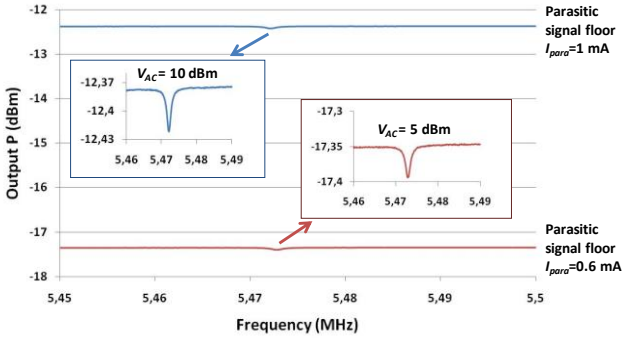

Figure 6: Output power versus frequency with input power of 5 dBm and 10 dBm (equals to V_{AC} of 0.6 V and 1V). (V_{DC}=3 V, Measurement bandwidth=100 Hz)

In order to obtain the resonance characteristic from the electrical measurement, one requires de-embedding the feedthrough signal (by subtracting the coupling signal floor in the real and imaginary part of the dynamic response respectively) to further process the data and extract the purely motional response (Figure 7).

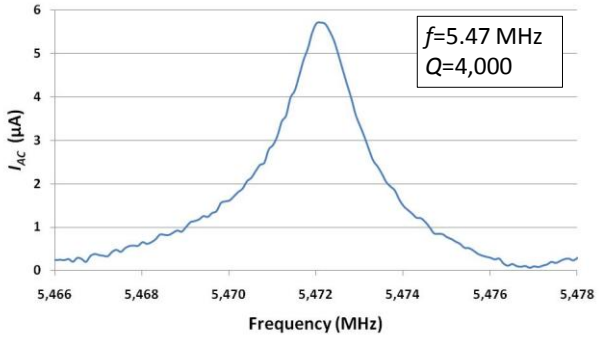

Figure 7: De-embedded piezoresistive current I_{AC} versus frequency with input power of 10 dBm. (V_{DC}=3 V, Measurement bandwidth=100 Hz)

After the de-embedded calculation, the quality factor of such device is found about 4,000 in air. Experimentally, it would be possible to retrieve purely resonance peak by using a frequency mixing technique or by canceling the coupling signal using an electronic nulling circuit which is currently under investigation.

Mechanical measurement of vibration amplitude

The mechanical measurement is performed on the same device in air using a MSA 500 Polytec Vibrometer. The laser beam is focused at the outer edge of heat tank of which the vibration amplitude is the same as that of the probe tip. Figure 8 shows the vibration amplitude versus frequency with different bias voltage V_{DC} of 3 V, 2 V, and 1 V. The corresponding vibration amplitude is 6.2 nm, 4 nm and 2 nm per V_{AC} respectively, which confirms the device linear functionality. The quality factor measured is about 4,000. The temperature fluctuation of such device is simulated (ANSYS) about 0.0125 K and the resonance frequency is slightly shifted to lower frequencies as V_{DC} increases due to the temperature dependent Young's modulus [10].

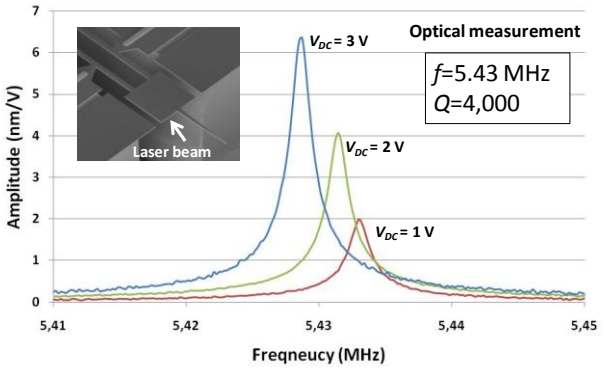

Figure 8: In-plane vibration amplitude (nm/V_{AC}) at tip location versus frequency with different bias voltage V_{DC}.

PROBE INTEGRATION AND AFM IMAGING

The dog-bone device is then mounted onto a commercial AFM set-up with a rigid probe holder (Figure 9). The supporting chip establishes the interconnections between dog-bone probe and the AFM control devices.

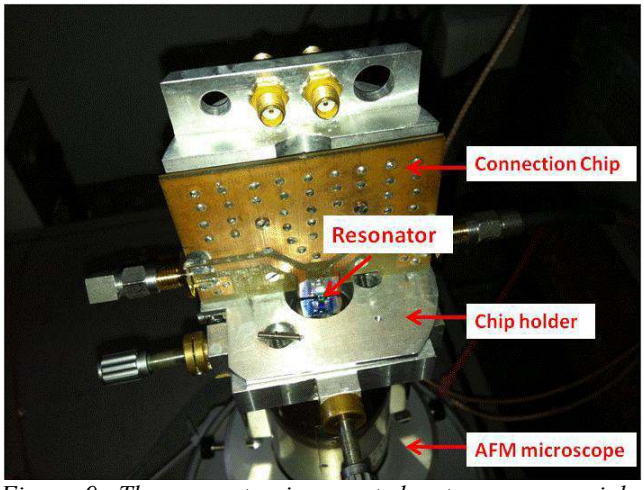

Figure 9: The resonator is mounted onto a commercial AFM microscope by using a dedicated circuit board.

Approach-retract curves

Figure 10 presents the output signal amplitude of the device versus tip-to-surface distance with a DC bias of 3 V and a 1.23 V AC driving voltage. The free oscillation amplitude (8nm) is estimated by measuring the extension of the intermittent contact regime which is consistent with the previous one obtained by laser vibrometry.

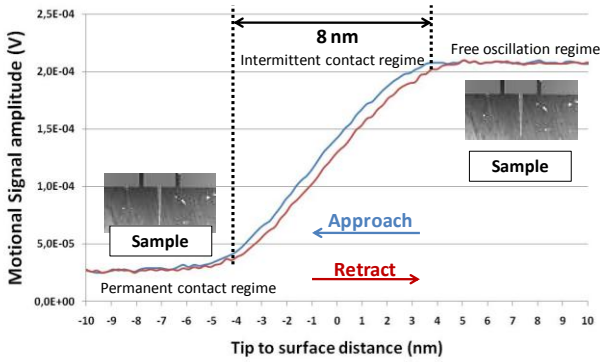

Figure 10: Probe signal amplitude as a function of the tip-to-surface distance. The probe is driven by a 3 V DC voltage and 1.23 V AC voltage.

Surface imaging

The probe is then used to scan over a 100 nm thick PMMA sample fabricated over a silicon substrate. Figure 11 shows two images acquired over the 2x2 µm sample pattern. Both images contain 512×512 pixels and the scanning speed is 20 µm/s. The topography is clearly defined with a resolution allowing distinguishing sample patterns and defects. By observing, such defect (on letters "M" and "N") is due to a strong tip-surface interaction during the scanning procedure.

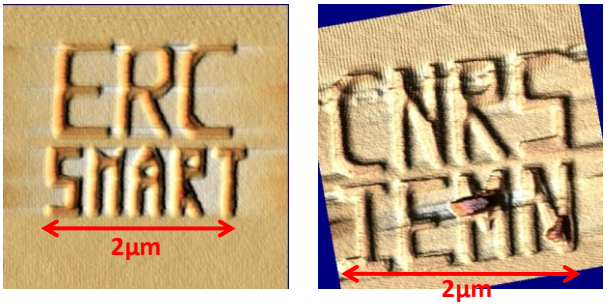

Figure 11: Sample surface AFM topographies obtained by the dog-bone probe working at 5.43 MHz with a scanning rate of 10 µm/s and acquisition time of 10 minutes.

By applying the calculation method presented in [4], the minimal detectable force can be estimated about 320 pN/ $Hz^{0.5}$.

Comparing to the F_{min} of our previous work (10 pN/ $Hz^{0.5}$ [5]) and of the commercial cantilever probe (several pN/ $Hz^{0.5}$), the current version dog-bone probe appears to be less sensitive in AFM imaging. Such characteristic can be explained as: first, the effective stiffness of longitudinal vibration structures is relatively larger than that of elliptic mode ring resonators and flexural mode cantilevers and the force sensitivity is thus limited. Second, the parasitic coupling masks the desired device signal and results in a low signal-to-noise ratio. Third, the device fabrication is based on uniformly doped silicon to avoid the temperature gradient created along the thickness which might result in unwanted vibration mode. Such feature is against the piezoresistive design concept and reduces the transduction efficiency. Using locally doped piezoresistors at maximum deformation location, that is to say, for the current device around the width edge of beams, the measurement sensitivity would be increased.

CONCLUSIONS AND FUTURE WORK

The possibility of using thermal-actuated and piezoresistive-sensed dog-bone resonator for AFM applications is demonstrated. The resonant frequency is measured at about 5.4 MHz and the quality factor is 4,000 in air. The probe is mounted onto a commercial AFM set-up and topographic images of PMMA sample are obtained. The force resolution deduced for the current probe is one order higher than our previous work on ring probe design. However, it is expected that using an optimal design with locally doped piezoresistors and by further processing the output signal, the force resolution could be significantly improved. Future work also considers AFM imaging in liquids, where the device would be coated by a thin isolation layer like SiN. It is expected that dog-bone probe would be then able to realize high speed/quality AFM images in liquid thanks to a favorable trade-off between transduction efficiency, stiffness and quality factor.

ACKNOWLEDGMENTS

The authors would like to acknowledge all the IEMN clean room and characterization center staff for their constant technical support. This work is funded by the European Research Council project "SMART" (ERC/SMART – Grant agreement n° 210078).

REFERENCES

[1] Ando, T. *et al. Progress in Surface Science*. **83**, pp 337-437, (2008)
[2] Faucher, M. *et al. Proc.Transducers'07,* pp. 1529-1532, (2007)
[3] Walter, B *et al. Journal of Micromechanics and Microengineering,* **19**, pp. 115001, (2009)
[4] Algre, E. *et al. Journal of Microelectromechical Systems,* **21**, pp. 385-397, (2012)
[5] Walter, B. *et al. Proc.MEMS2012,* pp 555-558, (2012)
[6] Xiong, Z. *et al. Proc.MEMS2012,* pp 547-550, (2012)
[7] Phan, K.L. *et al. Proc.Transducers'09,* pp. 1413-1416, (2009)
[8] Bontemps, J.J.M. *et al. Proc.Transducers'09,* pp.1433-1436, (2009)
[9] Amir, R. *et al. Transactions on Electron Devices,* **58**, pp. 1205-1214, (2011)
[10] Cho, C-H. *Current Applied Physics*, **9**, pp. 538-545, (2009)

CONTACT

Z. Xiong, zhuang.xiong@isen.iemn.univ-lille1.fr